Journal of Theoretical Biology 587 (2024) 111806

Contents lists available at ScienceDirect

Journal of Theoretical Biology

journal homepage: www.elsevier.com/locate/yjtbi

A resource-based mechanistic framework for castration-resistant prostate cancer (CRPC)

B. Vibishan [a], Harshavardhan B.V. [a,b], Sutirth Dey [a,*]

[a] Department of Biology, Indian Institute of Science Education and Research (IISER) Pune, Pune, Maharashtra, India
[b] IISc Mathematics Initiative, Indian Institute of Science, Bangalore, Karnataka, India

ARTICLE INFO

Keywords:
Prostate cancer
Tumour ecology
Resource consumption
Logistic growth
Community dynamics

ABSTRACT

Cancer therapy often leads to the selective elimination of drug-sensitive cells from the tumour. This can favour the growth of cells resistant to the therapeutic agent, ultimately causing a tumour relapse. Castration-resistant prostate cancer (CRPC) is a well-characterised instance of this phenomenon. In CRPC, after systemic androgen deprivation therapy (ADT), a subset of drug-resistant cancer cells autonomously produce testosterone, thus enabling tumour regrowth. A previous theoretical study has shown that such a tumour relapse can be delayed by inhibiting the growth of drug-resistant cells using biotic competition from drug-sensitive cells. In this context, the centrality of resource dynamics to intra-tumour competition in the CRPC system indicates clear scope for the construction of theoretical models that can explicitly incorporate the underlying mechanisms of tumour ecology. In the current study, we use a modified logistic framework to model cell–cell interactions in terms of the production and consumption of resources. Our results show that steady state composition of CRPC can be understood as a composite function of the availability and utilisation efficiency of two resources-oxygen and testosterone. In particular, we show that the effect of changing resource availability or use efficiency is conditioned by their general abundance regimes. Testosterone typically functions in trace amounts and thus affects steady state behaviour of the CRPC system differently from oxygen, which is usually available at higher levels. Our data thus indicate that explicit consideration of resource dynamics can produce novel and useful mechanistic understanding of CRPC. Furthermore, such a modelling approach also incorporates variables into the system's description that can be directly measured in a clinical context. This is therefore a promising avenue of research in cancer ecology that could lead to therapeutic approaches that are more clearly rooted in the biology of CRPC.

1. Introduction

Prostate cancer is among the leading causes of mortality in men (Cancer Society, 2023), and both its clinical progression and therapy have been the subject of intense theoretical investigation (Basanta et al., 2012; Zhang et al., 2017; Cunningham et al., 2018; West et al., 2020; Zhang et al., 2022). Research over the past few years has revealed an important role for intra-tumour competition in prostate cancer progression, particularly in drug-resistant relapse in advanced castration-resistant prostate cancer (CRPC) (Zhang et al., 2017; Gallaher et al., 2018; Brady-Nicholls et al., 2020). While intra-tumour competition is contingent on a diversity of cancer cell types occupying the tumour microenvironment (Gatenby et al., 2009; Kareva et al., 2015; Carreira et al., 2014; Gedye and Navani, 2022; Madan et al., 2022), such cellular heterogeneity also gains therapeutic relevance when a subset of cancer cells in the tumour are resistant to a given drug treatment. Investigations of such tumour populations comprised of a diversity of drug sensitivity phenotypes have demonstrated that drug-resistant relapse under conventional treatment approaches is primarily due to selective elimination of drug-sensitive cells from the tumour by therapy, which in turn allows drug-resistant cells to proliferate more freely (Gatenby et al., 2009; Marusyk et al., 2014; Sahoo et al., 2021; Farrokhian et al., 2022). Current research efforts are therefore aimed at the design of alternative therapeutic regimens that can prevent such competitive release of drug-resistant cells across a variety of cancer types (Hansen and Read, 2020; West et al., 2020).

Prostate cancer is well-characterised in terms of its clinical progression (Gordetsky and Epstein, 2016; Montironi et al., 2018) and the emergence of advanced castration-resistant prostate cancer (CRPC) is considered to be driven primarily by cancer cell types that are

* Corresponding author.
E-mail addresses: vibishan.b@students.iiserpune.ac.in (B. Vibishan), bv_harshavardhan@live.com (Harshavardhan B.V.), s.dey@iiserpune.ac.in (S. Dey).

https://doi.org/10.1016/j.jtbi.2024.111806
Received 18 September 2023; Received in revised form 4 February 2024; Accepted 25 March 2024
Available online 2 April 2024

resistant to chemical suppression of systemic androgen growth factors through androgen deprivation therapy (ADT) (Culig et al., 1999; Grasso et al., 2012; Fontana et al., 2022). In this context, progress towards alternative strategies to treat CRPC has focused on biotic interactions between androgen-dependent cells that are sensitive to ADT and androgen-independent cells that are resistant to ADT. The presence of such interactions is a key aspect of the development of intermittent androgen deprivation (IAD) therapies that are aimed at better managing drug resistance in a growing tumour (Phan et al., 2020; Pasetto et al., 2022). Much of this work builds either on compartment models of androgen-dependent and -independent cells in prostate cancer, or kinetic models of androgen metabolism (Hirata et al., 2018; Phan et al., 2020; Pasetto et al., 2022). On the other hand, more recent work has explicitly considered the role of androgen-producing cells in prostate cancer progression and the optimisation of fluctuating dosing strategies (Zhang et al., 2017; Cunningham et al., 2018). Producer cell types can drive tumour expansion by autonomous production of the androgen, testosterone, thus indirectly supporting the growth of androgen-dependent tumour cell types. This adds a commensal dimension to the existing competitive interactions in the system between producers and consumers of testosterone, while also making competition dynamics with androgen-independent cells more complex. Cell-autonomous production of testosterone could further drive the clinical progression of prostate cancer towards castration resistance by enabling tumour growth without systemic testosterone supply, which, as mentioned earlier, is directly relevant to the development of CRPC following androgen-deprivation therapy (ADT).

In an important study that includes tumour-internal androgen production, Cunningham et al. (2018) found that the interaction strengths between the cancer cell types, as described by the interaction coefficients, could be used to classify the dynamics and steady states of the model as “Best Responders”, “Responders” or “Non-responders”, to a drug that inhibits testosterone production. Only the testosterone-dependent cell types are sensitive to the inhibitory drug. Therefore, in absence of inter-conversion between these cell types through mutation, a higher frequency of the testosterone-independent cell type will lead to an increasingly drug-resistant tumour population. The relative steady-state frequencies of testosterone-dependent cell types therefore determines the “responsiveness” category to which the tumour population is assigned. For the Cunningham et al. model, the steady-state frequencies are largely determined by the configuration of various interaction coefficients, such that the stratification of model behaviour into responsiveness categories is essentially the identification of points in the interaction coefficient parameter space corresponding to qualitative differences in model dynamics. The roles of other ecologically-relevant factors like differences in intrinsic growth rates, initial population size, and initial population composition remain unclear.

The Cunningham et al. model represents the use of a classic ecological model of interspecific competition to functionalise tumour heterogeneity within a framework for therapeutic intervention in CRPC. While models of this kind provide valuable phenomenological insights into the progression of CRPC, it is difficult to relate their findings to physiological processes operating within a tumour community. Parameters like the interaction coefficients are usually not directly informative about the underlying mechanisms of cell–cell interactions, and the lack of direct mechanistic links to tumour processes could limit the translational applicability of such models.

Classical theoretical ecology, on the other hand, offers other conceptual frameworks that more explicitly account for the mechanisms of inter-specific interactions. Resource-consumer models represent one such framework within theoretical ecology that cast interspecific interactions entirely in terms of production, supply and consumption of, and competition for, physically explicit resources (Tilman, 1980; Grover, 1997; Muscarella and O’Dwyer, 2020). Their mechanistic roots arguably makes these models harder to parameterise than a logistic framework, which might explain their limited use in cancer systems so far (Kareva et al., 2015). Nevertheless, a resource dynamics based approach offers considerable potential to relate tumour ecology to measurable quantities within the tumour microenvironment.

In this study, we add a mechanistic element to the phenomenological description of the Cunningham et al. model by including the temporal dynamics of two resources-oxygen and testosterone. Oxygen, or the lack thereof (i.e. hypoxia), has been implicated in at least three separate cancer hallmarks including deregulated cellular energetics, angiogenesis, and metastasis (Hanahan and Weinberg, 2011), which makes it a biologically-pertinent inclusion in this model. As recognised by earlier work, testosterone is indispensable to any mechanistic description of the prostate tissue, cancerous or otherwise, as androgens are an integral part of prostate homeostasis (Mohler et al., 2004; Page et al., 2006; Calistro Alvarado, 2010). Furthermore, the demonstrated relevance of within-tumour testosterone production for the progression of advanced prostate cancer (Titus et al., 2005; Montgomery et al., 2008; Stanbrough et al., 2006; Watson et al., 2015) makes it a germane addition to the model.

The inclusion of resource dynamics in our model entails additional processes like cellular resource production and consumption that must be parameterised, and wherever possible, we have determined these parameter values based on available empirical measurements of the corresponding processes. Within this theoretical framework, our results enable us to construct an understanding of the steady state behaviour of the CRPC system in terms of the differential resource use properties of three distinct types of prostate cancer cells. Our data broadly demonstrate that resource consumption processes could potentially elucidate underlying mechanistic links within a system that is otherwise largely phenomenological. In particular, we find that the efficiency of resource use and abundance regimes of resources both play important roles in determining the steady-state composition of the tumour. We also identify resource use efficiency as an interesting aspect of tumour-intrinsic properties that could potentially be used to predict the sensitivity and responsiveness of a given tumour to testosterone-targeting therapy.

2. Methods

2.1. Model framework

Fig. 1 shows a schematic with the main components of the current model. Following the Cunningham et al. model, we use three separate logistic equations (Eq. (1)) with density-dependent competition to describe the dynamics of each of the three types of cancer cells: T^+, which requires testosterone for growth but cannot synthesise it; T^p, which also requires testosterone for growth but is capable of autonomous testosterone production; and T^-, which neither requires nor produces testosterone. We use two ODEs to describe the dynamics of two resources-oxygen (Eq. (2)) and testosterone (Eq. (3))-that contribute directly to cell growth (Fig. 1A).

In order to connect resource levels to cell abundances, we model the cell type-specific carrying capacities as dynamic functions of real-time resource levels according to their respective consumption modalities detailed further below, such that competitive interactions in the model are realised through the levels of each resource. The complete set of equations are as follows:

$$\frac{dy_i}{dt} = r_i\ y_i\ \left(1 - \frac{\sum_i y_i}{1 + K_{i,max}\ f_i(O_2)\ f_i(T)}\right) - \delta_i\ y_i,\ \text{for } i \in \{T^+,\ T^p,\ T^-\} \tag{1}$$

$$\frac{dO_2}{dt} = p_{O_2} - \sum_i \mu_{O_2,i}\ y_i - \lambda_{O_2} O_2,\ \text{for } i \in \{T^+,\ T^p,\ T^-\} \tag{2}$$

$$\frac{dT}{dt} = p_T\ y_{T^p} - \sum_i \mu_{T,i}\ y_i - \lambda_T T,\ \text{for } i \in \{T^+,\ T^p\} \tag{3}$$

where r_i, y_i and δ_i are the growth rate, abundance and death rate for cell type i, and p_j, $\mu_{j,\ i}$ and $\lambda_{j,\ i}$ are the production, consumption

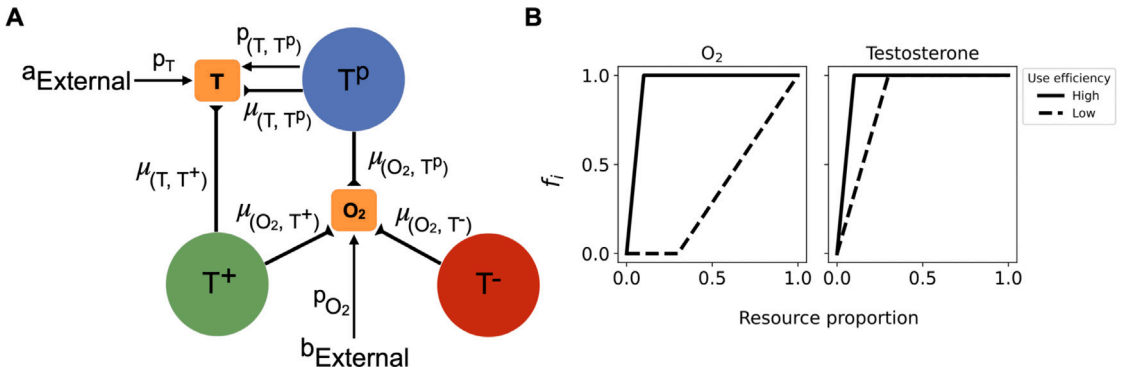

Fig. 1. Schematic showing the components of the current model. (A) Three cell types of CRPC, with oxygen as the common resource and testosterone (T) as the T^p-produced resource. Regular arrows indicate production of a resource and inverted arrowheads indicate consumption. Corresponding rates are given alongside the arrows. In general, μ is a consumption rate and p is a production rate. (B) Functional forms used to describe the two resource use efficiencies. See main text for descriptions of the cell types and resource use efficiencies. [a]External production of testosterone is turned off unless otherwise mentioned. [b]External production of oxygen is either low or high, but always non-zero.

and decay rates for cell type i and resource j. We model oxygen as a common resource that is supplied externally, at the constant rate p_{O_2}, in a cell-independent manner reflecting baseline blood supply. It is consumed by all three cell types and leaks out of the tumour tissue at some constant rate. Since castration-resistant prostate cancer arises after some period of androgen deprivation therapy (Mohler et al., 2004), we initially assume that there is no external supply of testosterone, such that any testosterone in the system is derived solely from production by T^p. As explained below, this is an assumption that we eventually relax to consider CRPC with external testosterone supply. Since T^- is testosterone-independent, testosterone consumption is only due to T^p and T^+, in addition to some constant leakage out of the tumour as with oxygen.

$K_{i,max}$ is the maximum carrying capacity for each cell type and this is further tuned by the availability of resources through the response function, $f_i(res)$. As a heuristic based on other models (Ghaffarizadeh et al., 2018), we assume f_i to be a piecewise linear function valued in [0, 1], such that it remains at zero for resource levels below a certain lower threshold value. Once the lower threshold is crossed, f_i increases linearly up to one at some upper threshold value, and stays at one thereafter. Fig. 1B shows the general shape of f_i for both resources and this is discussed further in the following section, but we note here that this form allows the effective carrying capacity, as represented by the whole of the denominator in Eq. (1), to respond dynamically to the amount of resources available in the environment. When $f_i(res) = 0$, the denominator is 1, and for abundant resource availability such that $f_i(res) = 1$, the denominator approaches $K_{i,max}$. The denominator also includes 1 to prevent division by zero under no availability of either or both resources. We choose 1 instead of adding a really small value (of the order of 10^{-12}) to prevent runaway errors over the course of numerical simulation.

2.2. Parameterisation and exploration

Table 1 gives a complete list of all the parameter values and their ranges used in the model. As noted above, we have tried to derive as many of these from empirical sources as possible, such that our model is rooted as far as possible in the biology of the system.

Growth and death rates for the cell types are in units of min^{-1} and derived from the doubling times of corresponding cell lines (see Table 1 and Supplementary Text). As the growth and death rates are different between the cell types, we derive $K_{i,max}$ for each cell type grown individually without resource limitations (i.e. $f_i(T) = f_i(O_2) = 1$) to achieve the same effective carrying capacity of 10 000 (Equation S2). We rescale all resource levels such that a resource level of 1 corresponds to the empirically measured steady state value of that resource in prostate cancer tissue. This enables us to sidestep a detailed treatment of the stoichiometry of two very different resources. Setting Eq. (2) to zero, we rescale empirically-derived cell-type specific consumption rates and decay rate for oxygen, and use these to calculate the steady state supply rate for oxygen assuming a population of only T^- cells. Similarly, setting Eq. (3) to zero, we use rescaled values of the production rate and natural decay rates for testosterone to calculate testosterone consumption rate for T^p. This rate is then used to determine the testosterone consumption rate for T^+. We restrict all equations to a biologically plausible space by requiring that $y_i = \frac{dy_i}{dt} = 0,\ if\ y_i < 1$ and only allowing non-zero population and resource abundances. Details of the parameterisation and normalisation are given in the Supplementary Text.

The efficiency of resource conversion into cellular growth is an important aspect of any resource-based conception of growth and competition. Resource efficiency is equally relevant to cancer, simply due to the diversity of niches and corresponding metabolic phenotypes within any solid tumour (Zheng, 2012; Birsoy et al., 2014; Loponte et al., 2019). Since environmental heterogeneity is well-documented in solid tumours, the availability and efficiency of use of oxygen could vary substantially between different regions of a tumour (Zheng, 2012). Similarly, variation has been identified across prostate cancer cell lines from several sources in their response to the availability and amount of testosterone in the system (Gregory et al., 2001; Chuu et al., 2011). Resource use efficiency could therefore underlie distinct metabolic strategies within a heterogeneous tumour population. We consider two distinct kinds of such metabolic strategies in our model for each resource, based on the use efficiency of each resource. We choose two distinct forms of the function f_i, corresponding to how much resource is required to realise the maximum carrying capacity in Eq. (2). The f_i for high use efficiency (Fig. 1B, solid line) reaches 1 at a lower resource level than that for low efficiency (Fig. 1B, dashed line), thus requiring a lesser amount of resource to realise maximum carrying capacity.

In addition to resource use, we also explore the effect of initial population size on the steady state composition of the system. This stems from the expectation that as the sole producer of testosterone, absolute abundance of T^p could have a significant impact on the balance of resource-based competition in the system.

All ODEs were simulated numerically using the LSODA algorithm through the `scipy.integrate.ode` function in Python, until a plateau was observed. Initial data suggested that a plateau was reached within $\sim$ 1000 days of model time for most parameter combinations. We therefore ran all simulations for 1000 days initially and subsequently extended the simulation time for those cases where a steady state had not been reached. Supplementary Figures S2–S5 show the time series for all the steady states examined in the main text along with the final run time in each case. All simulations reached steady state within 2500 days, except for only one combination of low oxygen use

Table 1
List of all parameters used in the current model. T stands for testosterone. Units of all resource-related parameters do not include dimensions of absolute abundance or concentration as these are normalised against res^*, and absolute values can be obtained by multiplying the parameter by res^*. Cell-type specific values of $K_{i,max}$ correspond to the value for which an effective carrying capacity of 10 000 is realised for that cell type growing without other competitors and abundant resource availability. Details of normalisation of resource parameters and derivation of growth parameters are given in the Supplementary Text. Supplementary Table S1 gives the values of empirically-derived rates and resource abundances used in the normalisation.

Parameter	Description	Value(s)			Source(s)
r_i	Population growth rate of cell type i		T^+	2.84×10^{-3} min^{-1}	Equation S1
			T^p	2.79×10^{-3} min^{-1}	
			T^-	6.23×10^{-4} min^{-1}	
δ_i	Population death rate of cell type i		T^+	2.5×10^{-3} min^{-1}	Jain et al. (2011)
			T^p	2.5×10^{-3} min^{-1}	
			T^-	1.6×10^{-4} min^{-1}	
$K_{i,max}$	Cell-type specific carrying capacity		T^+	8.35×10^4	Equation S2
			T^p	9.62×10^4	
			T^-	1.34×10^4	
p_{res}	Production rate of resource, either as bulk or by cells	O_2		0.11 min^{-1}	Equations S3 and S4
		T		5×10^{-7} min^{-1} cell^{-1}	
$\mu_{res,i}$	Uptake of resource res by cell type i	O_2	T^+	1.63×10^{-6} min^{-1} cell^{-1}	Hail et al. (2010), Equation S3
			T^p	1.63×10^{-6} min^{-1} cell^{-1}	
			T^-	1.04×10^{-6} min^{-1} cell^{-1}	
		T	T^+	2.34×10^{-8} min^{-1} cell^{-1}	
			T^p	6.00×10^{-8} min^{-1} cell^{-1}	
			T^-	0 min^{-1} cell^{-1}	
λ_{res}	Decay rate of resource	O_2		0.100 min^{-1}	Ghaffarizadeh et al. (2018) and Jain et al. (2011) and supplements therein
		T		0.004 min^{-1}	

efficiency and high testosterone use efficiency, and initial population size of 500, which was simulated for 5000 days. Custom Python scripts have been used for all the simulations, data analysis and plotting.

3. Results

Our model aims to investigate intra-tumour cell dynamics in CRPC in terms of the availability of and competition for resources. Specifically, we study the effects of changing resource availability under varying conditions of resource use efficiency and population size. Considering two distinct levels of supply for both oxygen and testosterone, we define four resource supply states under which we examine steady state tumour composition. The first state is when **neither** resource is supplemented externally, testosterone production is entirely from T^p, and oxygen supply is at a low level, as in a hypoxic tumour. In the second state, **only oxygen** is supplemented and we use a higher value of the oxygen supply rate, while testosterone production remains restricted to T^p. In the third state, there is **only testosterone** supplementation, implemented by the inclusion of a constant supply term independent of T^p in Eq. (3), while oxygen supply rate is low. In the fourth state, **both** resources are supplemented, oxygen supply rate is high, and external supply of testosterone is included.

We evaluate model outcomes based on whether or not T^p and T^+ are able to persist at steady state. In the context of therapy, we consider the competitive exclusion of the testosterone-dependent cell types by T^- an unfavourable outcome, the reasons for which will be discussed later. We classify model behaviour into four distinct tumour responses based on the particular resource supply state in which steady-state persistence of T^p and T^+ occurs. The first is a T-type response, which signifies that external supplementation of testosterone is sufficient for $T^p - T^+$ persistence at steady state. The second is an O-type response, which signifies that external supplementation of O_2 alone is sufficient for $T^p - T^+$ persistence. The third is a TO-type response signifying that external supplementation of both resources is required for $T^p - T^+$ persistence. The fourth response is called an N-type one, and indicates that $T^p - T^+$ persistence is not possible under any of the resource supply states tested here. Unless otherwise stated, all simulations are initialised with equal numbers of all three cell types and resource use efficiencies are identical across all three cell types. In the following sections, we illustrate how both resource use efficiency and supply states can play key roles in determining the overall tumour response as defined above.

3.1. Steady state composition under high resource use efficiency: a mix of tumour responses

Fig. 2 shows the steady-state composition of the tumour across the four resource supply states when both resources are used at the same efficiency, either both high (Fig. 2A) or both low (Fig. 2B). At high use efficiency (Fig. 2A), for any initial population size, $T^p - T^+$ are competitively excluded by T^- when neither resource is supplemented externally. This is intuitive as T^p and T^+ are dependent on both testosterone and oxygen for growth, and lack of external supplementation of both resources puts them at a competitive disadvantage relative to T^- which are limited only by oxygen. At population size 500, external supply of testosterone is sufficient to ensure $T^p - T^+$ persistence, indicating a T-type response. However, for higher initial population sizes, external supply of either or both resources can ensure $T^p - T^+$ persistence, suggesting a T- and O-type tumour response. Both these responses can be understood by identifying the limiting resource in each case. In the absence of external testosterone supply, T^p cells are the only source of testosterone in the system. A small initial population with few T^p cells and no external testosterone supply is therefore limited by testosterone, leading to a T-type tumour response. Larger initial population sizes also entail higher T^p frequency, thus relieving testosterone limitation. Under these circumstances, external supply of either one of the resources is sufficient to support $T^p - T^+$ growth and steady-state persistence. Taken together, our data indicate that high resource use efficiency generally favours $T^p - T^+$ persistence at steady state under a range of resource supply conditions, although this tendency is affected by the initial population size.

Under low use efficiency of both resources, Fig. 2B shows that supply of both resources is necessary for $T^p - T^+$ persistence at steady state, indicating a TO-type tumour response. Contrary to high efficiency (Fig. 2A), the TO-type response under low use efficiency is unaffected by the initial population size. We also observe that under low efficiency, low supply of oxygen leads to a smaller steady-state population size

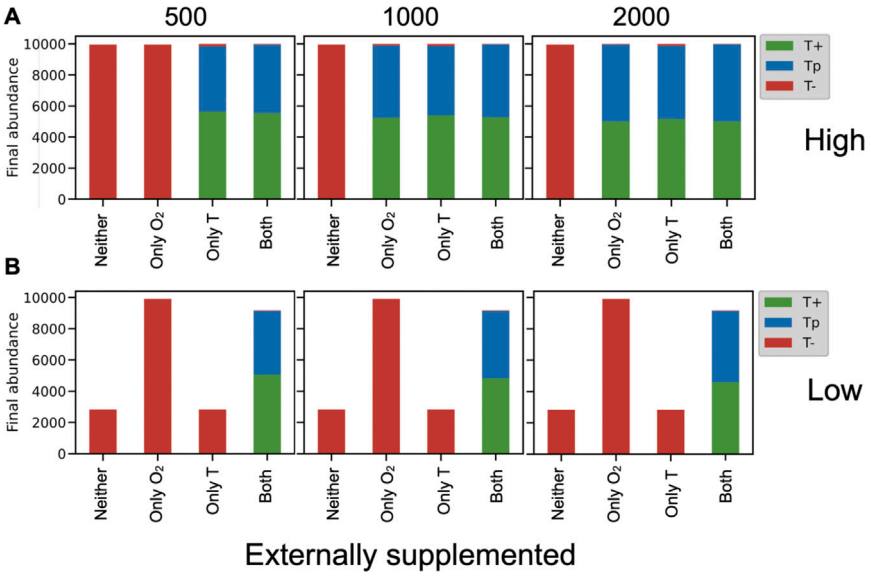

Fig. 2. Steady state behaviour under identical use efficiencies of both resources. Abundances of all three cell types, under (A) high use efficiency of both resources, and (B) low use efficiency of both resources; initial population sizes are given on top of each subpanel and equal numbers of each cell type were seeded in the beginning. Without external supplementation, $p_{O_2} = 0.06$ min^{-1}, O_2 at $t = 0$ was set to 0, and testosterone was produced by T^p at a rate $p_T = 5 \times 10^{-7}$ min^{-1} per cell. Under external supplementation, $p_{O_2} = 0.11$ min^{-1}, O_2 at $t = 0$ was set to 0.5 and an additional supply of 0.001 min^{-1} was added to Eq. (3). T at $t = 0$ was always 0. High use efficiency (i.e. panel A) usually leads to either a T- or T/O-type tumour response depending on the initial population size. Low use efficiency (i.e. panel B) produces an obligate TO-type tumour response regardless of initial population size. Further elaboration on tumour response types are in the main text.

while the lack of external testosterone supply does not have such an effect on the steady-state population size. This disparity is explicable based on the functional form of low use efficiency of oxygen, which allows only a fraction of the maximum carrying capacity to be realised under the oxygen-limiting conditions imposed by limited external supply. It is also worth noting that since testosterone use efficiency is also low, T^p–T^+ growth is limited strongly by both oxygen and testosterone at all times, and therefore requires external supplementation of both resources for their persistence. This leads to a TO-type response.

3.2. Mismatched resource use efficiencies reveal the lability of tumour responses

So far, we have only dealt with identical use efficiency of both resources — either both high or both low. We now consider responses to resource supplies of tumours with one resource used at high efficiency and the other at low efficiency. As Fig. 3 (left) shows, low testosterone use efficiency is the simpler of the two in terms of tumour responses, as it leads to an obligate T-type response. This implies that $T^p - T^+$ persistence requires external testosterone supply regardless of the initial population size, and as Fig. 3A, C and E make clear, testosterone is both necessary and sufficient for $T^p - T^+$ persistence. As observed earlier, lower testosterone abundance does not affect the steady state population size.

Low use efficiency of oxygen coupled with high testosterone use efficiency presents a more complicated picture. As shown in Fig. 3 (panels B, D and F), steady state population size responds to low oxygen abundance as expected, leading to a smaller final population. However, when oxygen and/or testosterone are supplied, tumour responses in terms of steady state composition show a greater degree of variability. Following the trend across Fig. 3B, D and F from top to bottom, at small initial population size (Fig. 3B), the lower frequency of T^p cells leads to testosterone limitation and the tumour shows a T-type response. Given that $T^p - T^+$ are already limited by testosterone, external supply of oxygen under small initial population size favours T^-. Intermediate initial population size increases the T^p frequency, but in the absence of external testosterone supply, testosterone production by T^p alone is insufficient for $T^p - T^+$ persistence. Since oxygen is already limiting, this leads to a TO-type response overall (Fig. 3D). Further increase in the initial population size increases T^p frequency, and this increase ameliorates the initial testosterone limitation. However, higher total cell number under low oxygen use efficiency makes oxygen the limiting resource in turn, and this leads to an O-type response (Fig. 3F). Low use efficiency of oxygen therefore reveals the potential for population size to determine which resource is actually limiting and how tumour populations respond to resource supply states.

3.3. Oxygen supply rate could affect producer–consumer cell abundance balance

Fig. 4 shows part of a finer exploration of the resource-supply parameter space, in which we vary the supply rates of both resources over a range of values. Under low use efficiency of only oxygen (Fig. 4A), we find that increasing the supply rate of oxygen increases the proportion of T^+ at steady state relative to T^p (*cf* Fig. 4A and B). Low efficiency use of testosterone, on the other hand, limits the viable resource supply region, such that population growth occurs for only the highest testosterone supply rate when its use efficiency is low (Fig. 4B; note that the x-axis here has only the highest value of testosterone supply rate). It is also worth noting that in the supply cases shown here, the steady-state population is almost entirely comprised of T^p and T^+, indicating that under sufficient resource abundance, T^- is competitively excluded. As further elucidated in Supplementary Figure S6, below some lower threshold supply rates of oxygen and testosterone, $T^p - T^+$ are both driven to extinction at steady state. While the data are not shown here, we also find that below some other threshold supply of oxygen lower still, all three cell types are driven to extinction. Testosterone supply and its use efficiency therefore seem to result in binary outcomes in terms of steady-state $T^p - T^+$ persistence. On the other hand, under conditions when testosterone availability is sufficient for $T^p - T^+$ persistence, higher oxygen availability favours a greater proportion of T^+ at steady state.

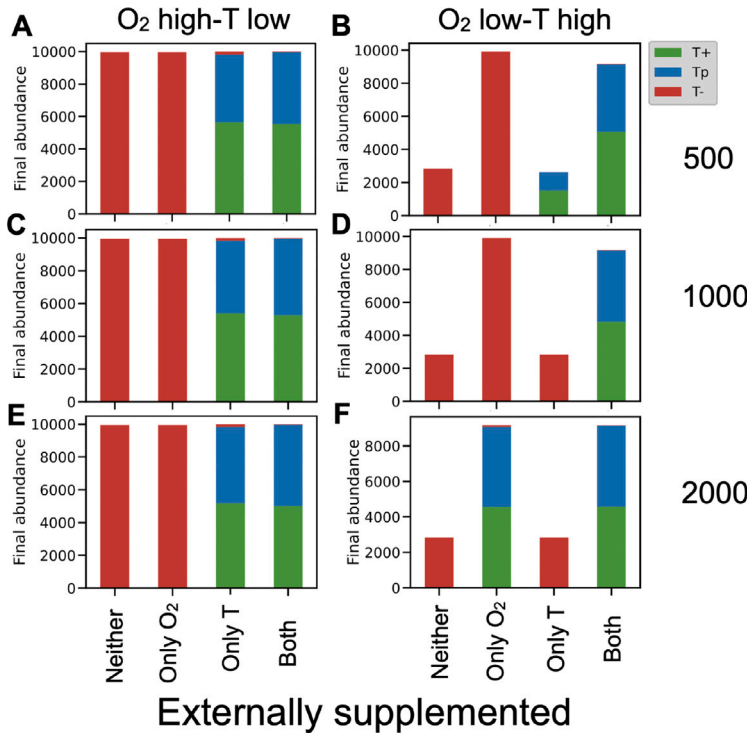

Fig. 3. Steady state behaviour under mismatched resource use efficiencies. Abundances of all three cell for (A, C, E) low use efficiency of testosterone only and (B, D, F) low use efficiency of oxygen only; initial population sizes vary across rows as given on the right end of each row, and equal numbers of each cell type were seeded in the beginning. Resource supplies were parameterised as mentioned earlier. T stands for testosterone. When testosterone use efficiency is low (A, C, E), tumour responses are obligately T-type regardless of initial population size. On the other hand, low use efficiency of oxygen (B, D, F) leads to shifting tumour responses, from T-type for small initial population size (B), to TO-type response (D), to an O-type response (F). See main text for further explanation.

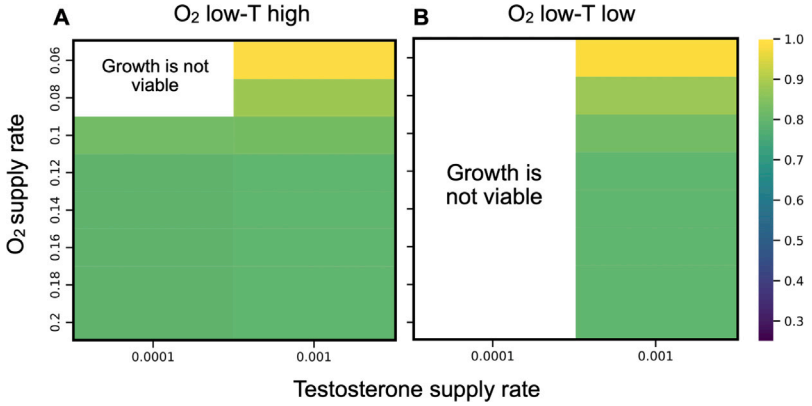

Fig. 4. Producer–consumer balance with varying oxygen supply. Steady state ratio of T^p against T^+ across a range of supply rates of oxygen and testosterone for low use efficiency of oxygen and either (A) high use efficiency or (B) low use efficiency of testosterone. Note that lower supply rates of either resource, below 0.0001 min^{-1} for testosterone and below 0.06 min^{-1} for oxygen, could not support any cell growth at all and are therefore not shown here. Empty spaces marked as "Growth is not viable" are resource supply states for which T^p and T^+ both go extinct. Oxygen supply rates on the y-axis increase from top to bottom. In all cases, simulations were initialised with equal numbers of all three cell types, with an initial population size of 500 and run for 2500 days.

3.4. Oxygen and testosterone function at different abundance regimes

The previous sections show that across resource efficiencies, oxygen and testosterone have qualitatively different effects on steady state population sizes and tumour compositions. To investigate these differences in further detail, we show part of the parameter exploration for the choice of upper and lower thresholds for $f_i(O_2)$ and $f_i(T)$ in Fig. 5A–B, for a population of T^p cells alone. The heat maps clearly demonstrate that when testosterone is only produced by T^p and oxygen is supplied externally, T^p growth is viable across the whole parameter space of upper and lower thresholds for oxygen (Fig. 5A). However, T^p goes extinct for testosterone lower thresholds of 0.2 or greater (Fig. 5B). Comparing this with a representative simulated time series of resource levels in Fig. 5C, we see that in the initial few days, testosterone levels remain slightly below 0.2 whereas oxygen levels increase rapidly to stabilise close to one. This distinction in turn stems from the fact that oxygen and testosterone are produced and consumed at vastly different rates in the system, leading to different abundances at steady state as well as different dynamics towards the steady state. Fig. 5 altogether demonstrates that the difference in steady state resource abundance corresponds to the parameter space of $f_i(O_2)$ and $f_i(T)$ where cell growth is viable. The extent to which the upper and lower thresholds can be varied for $f_i(T)$ is therefore much more restricted than for $f_i(O_2)$, primarily due to differences in the underlying resource dynamics.

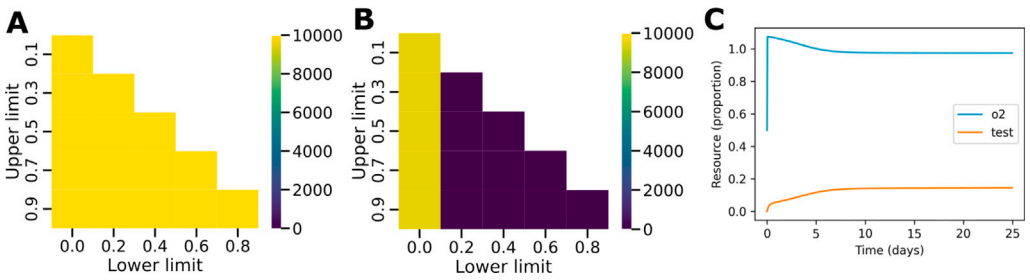

Fig. 5. Abundance regimes of oxygen vs. testosterone. Steady state abundances of a population of T^p cells grown without resource limitation and in the absence of other cell types, under a range of thresholds for f_i of (A) oxygen and (B) testosterone, and (C) representative time series of resource dynamics in the first 25 days. For panels (A) and (B), upper and lower threshold values correspond to the upper and lower inflection points of f_i as shown in Fig. 1B. The missing upper diagonal values of (A) and (B) are not valid threshold values of f_i as the lower limit must be less than the upper limit by definition. For (C), equal numbers of all three cell types were initialised, initial total population size was 2000, lower and upper thresholds were 0 and 1 respectively for $f_i(O_2)$, 0 and 0.1 for $f_{T^p}(T)$, and 0 and 0.05 for $f_{T^+}(T)$, and $p_{O_2} = 0.11$ min^{-1}.

4. Discussion

Androgen dependence has been a much-studied aspect of prostate cancer in the context of progression of castration-resistant growth (reviewed in Phan et al., 2020; Pasetto et al., 2022). The current study goes beyond previous investigations (Cunningham et al., 2018) by allowing us to describe system behaviour in terms of the availability and consumption of resources that are pertinent to the biology of CRPC. In the absence of external supplementation, oxygen in our model is usually present at much higher levels than testosterone (Fig. 5), which is consistent with measurements from the tumour microenvironment (Dillard et al., 2008; Stewart et al., 2010). As T^p and T^+ are simultaneously limited by two resources, they are driven to extinction in many parts of the resource efficiency-supply space (Figs. 2 and 3). While low resource use efficiency is detrimental to $T^p - T^+$ survival overall (Fig. 2B), overcoming this through external supply of the limiting resource is context-dependent. Fig. 3A shows that when testosterone use efficiency is low, external supply of testosterone is always sufficient to ensure $T^p - T^+$ survival. When oxygen use efficiency is low, Fig. 3B shows that the initial population size determines which resource is limiting and can therefore support $T^p - T^+$ survival if supplied externally. Fig. 4 shows a specific part of the resource supply-efficiency parameter space in which oxygen supply seemingly favours a higher abundance of T^+ at steady state. Since T^+ has a slightly higher doubling rate than T^p, it is possible that its growth could be favoured by the presence of higher resource abundance.

On the whole, our data suggest that resource use efficiencies could serve as potential tumour-intrinsic properties that could be predictive of tumour composition at steady state. In the case of CRPC, the steady-state composition serves as an indicator of whether the tumour is likely to respond to resource-targeting therapy. As T^p and T^+ are both testosterone-dependent cell types, their persistence at steady state leads to a tumour that would respond to testosterone inhibition. On the other hand, a higher frequency of T^- at steady state leads to a tumour that is less responsive to testosterone-targeting therapy as T^- cells are not dependent on testosterone for growth. Given that the development of personalised cancer therapy is a subject of active research (Martin et al., 2015; Hansen et al., 2017; Marigorta et al., 2017; Gedye and Navani, 2022), our data indicate that the elucidation of resource use strategies in a tumour could form the basis of designing more effective, personalised therapeutic strategies for CRPC cases depending on the extent of resource dependencies within the tumour. We also speculate that the abundance regime in which a resource operates could be an important factor in determining its therapeutic relevance. Testosterone in our model operates at a much lower abundance than oxygen. On one hand, this identifies testosterone as a clear target for therapeutic approaches involving resource supply as it is invariably limiting. However, we also find that model behaviour is highly sensitive to changes in testosterone availability, with very sharp thresholds for steady-state $T^p - T^+$ persistence (Supplementary Figure S6). To what extent these thresholds are an artefact of our parameterisation of resource use efficiencies is unclear, and this is a subject of ongoing investigation.

Although we use clinically relevant parameter regimes for our data, our model results have not been fit to longitudinal data from patient samples, unlike some other models in this context (Hirata et al., 2018; Foryś et al., 2022; Zhang et al., 2022). Consequently, rather than providing precise quantitative predictions about the progression and dynamics of CRPC, our results point towards qualitative patterns and behaviours of such a system. One such observation from the model relates to cases where drug sensitivity is accompanied by unique resource use strategies. Under such conditions, the external supply of resources used specifically by sensitive cells supports their growth, while drug treatment retards their growth. This suggests that resource supply, due to its effect on intra-tumour competition, could potentially be used as a counterweight to chemotherapy to extend the time for which the tumour responds to the therapy. A recent resource-consumer model of estrogen and glucose consumption in breast cancer has used an R^*-based conceptual framework to demonstrate effects of resource dynamics on intra-tumour competition in the absence of chemotherapy (Kareva and Brown, 2021). Furthermore, tumours of an LNCaP-derived cell line when implanted in athymic mice have been shown to undergo significant regression and necrosis when the mouse is given a testosterone bolus (Umekita et al., 1996). Therapeutic use of testosterone also offers the possibility of improvements in patient-reported Quality of Life indicators that are typically adversely affected by prolonged androgen deprivation (Niraula et al., 2016). More generally, our data indicate that a theoretical framework that integrates available information on the biology of resource use in a tumour with its growth dynamics could considerably expand our current toolkit for cancer control. This could be particularly relevant for endocrine cancers, most of which frequently have a hormone or growth factor signalling axis that is crucial for cancer progression, as exemplified by the importance of EGFR signalling in breast cancer (Osborne et al., 1985; Kareva and Brown, 2021), testosterone signalling in prostate cancer (Mohler et al., 2004), or insulin signalling in pancreatic cancer (Chan et al., 2014; Archetti et al., 2015).

Realising the translational value of resource use models in cancer treatment depends on the ability to identify and monitor relevant cellular phenotypes and resource availability. One potentially interesting avenue are the so-called "radiomics" approaches that can integrate quantitative imaging data with additional information about spatial structure, genomics and gene expression to help with diagnosis and monitoring (Gillies et al., 2016). Such analyses have been applied to classify prostate cancer and benign masses accurately, and further separate different kinds of tumours with the same overall Gleason score (3 + 4 vs. 4 + 3, for example Wibmer et al. (2015) and Fehr et al. (2015)). The possibility of obtaining such information before and after a therapeutic intervention represents unprecedented scope in the future for precise, patient-driven treatment that can respond to drug-induced ecological and evolutionary changes in a tumour. Theoretical

models must therefore be geared to make use of such granular data from the tumour microenvironment to enable an ecologically-informed treatment approach.

CRediT authorship contribution statement

B. Vibishan: Conceptualization, Formal analysis, Investigation, Methodology, Visualization, Writing – original draft, Writing – review & editing. **Harshavardhan B.V.:** Formal analysis, Investigation, Methodology, Software, Visualization, Writing – review & editing. **Sutirth Dey:** Conceptualization, Funding acquisition, Project administration, Resources, Supervision, Writing – review & editing.

Declaration of competing interest

The authors declare that they have no known competing financial interests or personal relationships that could have appeared to influence the work reported in this paper.

Acknowledgements

The authors acknowledge current and past members, and visiting students of the Population Biology Lab at IISER Pune for extensive critical inputs on previous analyses. The authors also thank Deepak Barua for useful discussions. This project was supported by grant # STR/2021/000021 from Science and Engineering Research Board, Department of Science and Technology (DST), Government of India and internal funding from Indian Institute of Science Education and Research (IISER), Pune, India. BV was supported by IISER Pune and HBV through the Kishore Vaigyanik Protsahan Yojana (KVPY), DST, Government of India.

Appendix A. Supplementary data

Supplementary material related to this article can be found online at https://doi.org/10.1016/j.jtbi.2024.111806.

References

Archetti, M., Ferraro, D.A., Christofori, G., 2015. Heterogeneity for IGF-II production maintained by public goods dynamics in neuroendocrine pancreatic cancer. Proc. Natl. Acad. Sci. U S A 112, 1–6. http://dx.doi.org/10.1073/pnas.1414653112, arXiv:1408.1149,

Basanta, D., Scott, J.G., Fishman, M.N., Ayala, G., Hayward, S.W., Anderson, A.R.A., 2012. Investigating prostate cancer tumour–stroma interactions: clinical and biological insights from an evolutionary game. Br. J. Cancer 106 (1), 174–181. http://dx.doi.org/10.1038/bjc.2011.517, Number: 1 Publisher: Nature Publishing Group.

Birsoy, K., Possemato, R., Lorbeer, F.K., Bayraktar, E.C., Thiru, P., Yucel, B., Wang, T., Chen, W.W., Clish, C.B., Sabatini, D.M., 2014. Metabolic determinants of cancer cell sensitivity to glucose limitation and biguanides. Nature 508 (1), 108–112. http://dx.doi.org/10.1038/nature13110, arXiv: NIHMS150003 Publisher: Nature Publishing Group ISBN: 1476-4687 (Electronic)–r0028-0836 (Linking).

Brady-Nicholls, R., Nagy, J.D., Gerke, T.A., Zhang, T., Wang, A.Z., Zhang, J., Gatenby, R.A., Enderling, H., 2020. Prostate-specific antigen dynamics predict individual responses to intermittent androgen deprivation. Nature Commun. 11 (1), 1750. http://dx.doi.org/10.1038/s41467-020-15424-4, Number: 1 Publisher: Nature Publishing Group.

Calistro Alvarado, L., 2010. Population differences in the testosterone levels of young men are associated with prostate cancer disparities in older men. Am. J. Human Biol. 22 (4), 449–455. http://dx.doi.org/10.1002/ajhb.21016, _eprint: https://onlinelibrary.wiley.com/doi/pdf/10.1002/ajhb.21016.

Cancer Society, A., 2023. Cancer Facts & Figures 2023. Am. Cancer Soc..

Carreira, S., Romanel, A., Goodall, J., Grist, E., Ferraldeschi, R., Miranda, S., Prandi, D., Lorente, D., Frenel, J.-S., Pezaro, C., Omlin, A., Rodrigues, D.N., Flohr, P., Tunariu, N., S. de Bono, J., Demichelis, F., Attard, G., 2014. Tumor clone dynamics in lethal prostate cancer. Sci. Transl. Med. 6 (254), 254ra125. http://dx.doi.org/10.1126/scitranslmed.3009448, Publisher: American Association for the Advancement of Science.

Chan, M.T., Lim, G.E., Skovsø, S., Yang, Y.H.C., Albrecht, T., Alejandro, E.U., Hoesli, C.A., Piret, J.M., Warnock, G.L., Johnson, J.D., 2014. Effects of insulin on human pancreatic cancer progression modeled in vitro. BMC Cancer 14, 814. http://dx.doi.org/10.1186/1471-2407-14-814, publisher: BioMed Central ISBN: 1471-2407 (Electronic)\r1471-2407 (Linking).

Chuu, C.-P., Kokontis, J.M., Hiipakka, R.A., Fukuchi, J., Lin, H.-P., Lin, C.-Y., Huo, C., Su, L.-C., Liao, S., 2011. Androgen suppresses proliferation of castration-resistant LNCaP 104-R2 prostate cancer cells through androgen receptor, Skp2, and c-Myc. Cancer Sci. 102 (11), 2022–2028. http://dx.doi.org/10.1111/j.1349-7006.2011.02043.x, _eprint: https://onlinelibrary.wiley.com/doi/pdf/10.1111/j.1349-7006.2011.02043.x.

Culig, Z., Hoffmann, J., Erdel, M., Eder, I.E., Hobisch, A., Hittmair, A., Bartsch, G., Utermann, G., Schneider, M.R., Parczyk, K., Klocker, H., 1999. Switch from antagonist to agonist of the androgen receptor blocker bicalutamide is associated with prostate tumour progression in a new model system. Br. J. Cancer 81 (2), 242–251. http://dx.doi.org/10.1038/sj.bjc.6690684, Number: 2 Publisher: Nature Publishing Group.

Cunningham, J.J., Brown, J.S., Gatenby, R.A., Staňková, K., 2018. Optimal control to develop therapeutic strategies for metastatic castrate resistant prostate cancer. J. Theoret. Biol. 459, 67–78. http://dx.doi.org/10.1016/j.jtbi.2018.09.022, Publisher: Academic Press.

Dillard, P.R., Lin, M.-F., Khan, S.A., 2008. Androgen-independent prostate cancer cells acquire the complete steroidogenic potential of synthesizing testosterone from cholesterol. Mol. Cell. Endocrinol. 295 (1), 115–120. http://dx.doi.org/10.1016/j.mce.2008.08.013.

Farrokhian, N., Maltas, J., Dinh, M., Durmaz, A., Ellsworth, P., Hitomi, M., McClure, E., Marusyk, A., Kaznatcheev, A., Scott, J.G., 2022. Measuring competitive exclusion in non–small cell lung cancer. Sci. Adv. 8 (26), eabm7212. http://dx.doi.org/10.1126/sciadv.abm7212, Publisher: American Association for the Advancement of Science.

Fehr, D., Veeraraghavan, H., Wibmer, A., Gondo, T., Matsumoto, K., Vargas, H.A., Sala, E., Hricak, H., Deasy, J.O., 2015. Automatic classification of prostate cancer Gleason scores from multiparametric magnetic resonance images. Proc. Natl. Acad. Sci. 112 (46), E6265–E6273. http://dx.doi.org/10.1073/pnas.1505935112.

Fontana, F., Anselmi, M., Limonta, P., 2022. Molecular mechanisms and genetic alterations in prostate cancer: From diagnosis to targeted therapy. Cancer Lett. 534, 215619. http://dx.doi.org/10.1016/j.canlet.2022.215619.

Foryś, U., Nahshony, A., Elishmereni, M., 2022. Mathematical model of hormone sensitive prostate cancer treatment using leuprolide: A small step towards personalization. PLoS ONE 17 (2), e0263648. http://dx.doi.org/10.1371/journal.pone.0263648.

Gallaher, J.A., Enriquez-Navas, P.M., Luddy, K.A., Gatenby, R.A., Anderson, A.R., 2018. Spatial heterogeneity and evolutionary dynamics modulate time to recurrence in continuous and adaptive cancer therapies. Cancer Res. 78 (8), 2127–2139. http://dx.doi.org/10.1158/0008-5472.CAN-17-2649, Publisher: American Association for Cancer Research.

Gatenby, R.A., Silva, A.S., Gillies, R.J., Frieden, B.R., 2009. Adaptive therapy. Cancer Res. 69 (11), 4894–4903. http://dx.doi.org/10.1158/0008-5472.CAN-08-3658.

Gedye, C., Navani, V., 2022. Find the path of least resistance: Adaptive therapy to delay treatment failure and improve outcomes. Biochimica et Biophysica Acta (BBA) - Rev. Cancer 1877 (2), 188681. http://dx.doi.org/10.1016/J.BBCAN.2022.188681, Publisher: Elsevier.

Ghaffarizadeh, A., Heiland, R., Friedman, S.H., Mumenthaler, S.M., Macklin, P., 2018. PhysiCell: An open source physics-based cell simulator for 3-D multicellular systems. In: Poisot, T. (Ed.), PLoS Comput. Biol. 14 (2), e1005991. http://dx.doi.org/10.1371/journal.pcbi.1005991, Publisher: Public Library of Science.

Gillies, R.J., Kinahan, P.E., Hricak, H., 2016. Radiomics: Images are more than pictures, they are data. Radiology 278 (2), 563–577. http://dx.doi.org/10.1148/radiol.2015151169, Publisher: Radiological Society of North America.

Gordetsky, J., Epstein, J., 2016. Grading of prostatic adenocarcinoma: current state and prognostic implications. Diagn. Pathol. 11 (1), 25. http://dx.doi.org/10.1186/s13000-016-0478-2.

Grasso, C.S., Wu, Y.-M., Robinson, D.R., Cao, X., Dhanasekaran, S.M., Khan, A.P., Quist, M.J., Jing, X., Lonigro, R.J., Brenner, J.C., Asangani, I.A., Ateeq, B., Chun, S.Y., Siddiqui, J., Sam, L., Anstett, M., Mehra, R., Prensner, J.R., Palanisamy, N., Ryslik, G.A., Vandin, F., Raphael, B.J., Kunju, L.P., Rhodes, D.R., Pienta, K.J., Chinnaiyan, A.M., Tomlins, S.A., 2012. The mutational landscape of lethal castration-resistant prostate cancer. Nature 487 (7406), 239–243. http://dx.doi.org/10.1038/nature11125, Number: 7406 Publisher: Nature Publishing Group.

Gregory, C.W., Johnson, R.T., Mohler, J.L., French, F.S., Wilson, E.M., 2001. Androgen receptor stabilization in recurrent prostate cancer is associated with hypersensitivity to low androgen. Cancer Res. 61 (7), 2892–2898.

Grover, J.P., 1997. Resource Competition. Springer Science & Business Media, Google-Books-ID: x89Rl1nYR8gC.

Hail, N., Chen, P., Bushman, L.R., 2010. Teriflunomide (leflunomide) promotes cytostatic, antioxidant, and apoptotic effects in transformed prostate epithelial cells: Evidence supporting a role for teriflunomide in prostate cancer Chemoprevention. Neoplasia 12 (6), 464–475. http://dx.doi.org/10.1593/neo.10168.

Hanahan, D., Weinberg, R.A., 2011. Hallmarks of Cancer: The next generation. Cell 144 (5), 646–674. http://dx.doi.org/10.1016/j.cell.2011.02.013.

Hansen, E., Read, A.F., 2020. Cancer therapy: Attempt cure or manage drug resistance? Evol. Appl. 13 (7), 1660–1672. http://dx.doi.org/10.1111/eva.12994, Publisher: Wiley.

Hansen, E., Woods, R.J., Read, A.F., 2017. How to use a chemotherapeutic agent when resistance to it threatens the patient. In: Schneider, D. (Ed.), PLOS Biol. 15 (2), e2001110. http://dx.doi.org/10.1371/journal.pbio.2001110, Publisher: Public Library of Science.

Hirata, Y., Morino, K., Akakura, K., Higano, C.S., Aihara, K., 2018. Personalizing androgen suppression for prostate cancer using mathematical modeling. Sci. Rep. 8, 2673. http://dx.doi.org/10.1038/s41598-018-20788-1.

Jain, H.V., Clinton, S.K., Bhinder, A., Friedman, A., 2011. Mathematical modeling of prostate cancer progression in response to androgen ablation therapy. Proc. Natl. Acad. Sci. 108 (49), 19701–19706. http://dx.doi.org/10.1073/pnas.1115750108, Publisher: National Academy of Sciences ISBN: 1091-6490 (Electronic)–r0027-8424 (Linking).

Kareva, I., Brown, J.S., 2021. Estrogen as an essential resource and the coexistence of ER+ and ER– cancer cells. Front. Ecol. Evol. 9.

Kareva, I., Morin, B., Castillo-Chavez, C., 2015. Resource consumption, sustainability, and cancer. Bull. Math. Biol. 77 (2), 319–338. http://dx.doi.org/10.1007/S11538-014-9983-1/FIGURES/4, Publisher: Springer Science and Business Media, LLC.

Loponte, S., Lovisa, S., Deem, A.K., Carugo, A., Viale, A., 2019. The many facets of tumor heterogeneity: Is metabolism lagging behind? Cancers 11 (10), 1574. http://dx.doi.org/10.3390/cancers11101574, Number: 10 Publisher: Multidisciplinary Digital Publishing Institute.

Madan, E., Palma, A.M., Vudatha, V., Trevino, J.G., Natarajan, K.N., Winn, R.A., Won, K.J., Graham, T.A., Drapkin, R., McDonald, S.A., Fisher, P.B., Gogna, R., 2022. Cell competition in carcinogenesis. Cancer Res. 82 (24), 4487–4496. http://dx.doi.org/10.1158/0008-5472.CAN-22-2217.

Marigorta, U.M., Denson, L.A., Hyams, J.S., Mondal, K., Prince, J., Walters, T.D., Griffiths, A., Noe, J.D., Crandall, W.V., Rosh, J.R., Mack, D.R., Kellermayer, R., Heyman, M.B., Baker, S.S., Stephens, M.C., Baldassano, R.N., Markowitz, J.F., Kim, M.-O., Dubinsky, M.C., Cho, J., Aronow, B.J., Kugathasan, S., Gibson, G., 2017. Transcriptional risk scores link GWAS to eQTLs and predict complications in Crohn's disease. Nature Genet. http://dx.doi.org/10.1038/ng.3936.

Martin, S.D., Coukos, G., Holt, R.A., Nelson, B.H., 2015. Targeting the undruggable: immunotherapy meets personalized oncology in the genomic era. Ann. Oncol. : Off. J. Euro. Soc. Med. Oncol. / ESMO 26 (12), 2367–2374. http://dx.doi.org/10.1093/annonc/mdv382.

Marusyk, A., Tabassum, D.P., Altrock, P.M., Almendro, V., Michor, F., Polyak, K., 2014. Non-cell-autonomous driving of tumour growth supports sub-clonal heterogeneity. Nature 514 (7520), 54–58. http://dx.doi.org/10.1038/nature13556, Number: 7520 Publisher: Nature Publishing Group.

Mohler, J.L., Gregory, C.W., Ford, III, O.H., Kim, D., Weaver, C.M., Petrusz, P., Wilson, E.M., French, F.S., 2004. The androgen axis in recurrent prostate cancer. Clin. Cancer Res. 10 (2), 440–448. http://dx.doi.org/10.1158/1078-0432.CCR-1146-03.

Montgomery, R.B., Mostaghel, E.A., Vessella, R., Hess, D.L., Kalhorn, T.F., Higano, C.S., True, L.D., Nelson, P.S., 2008. Maintenance of intratumoral androgens in metastatic prostate cancer: A mechanism for castration-resistant tumor growth. Cancer Res. 68 (11), 4447–4454. http://dx.doi.org/10.1158/0008-5472.CAN-08-0249.

Montironi, R., Cimadamore, A., Cheng, L., Lopez-Beltran, A., Scarpelli, M., 2018. Prostate cancer grading in 2018: limitations, implementations, cribriform morphology, and biological markers. Int. J. Biol. Markers 33 (4), 331–334. http://dx.doi.org/10.1177/1724600818781296, Publisher: SAGE Publications Ltd STM.

Muscarella, M.E., O'Dwyer, J.P., 2020. Species dynamics and interactions via metabolically informed consumer-resource models. Theor. Ecol. 13 (4), 503–518. http://dx.doi.org/10.1007/s12080-020-00466-7.

Niraula, S., Templeton, A.J., Vera-Badillo, F.E., Joshua, A.M., Sridhar, S.S., Cheung, P.W., Yip, P.M., Dodd, A., Nugent, Z., Tannock, I.F., 2016. Study of testosterone-guided androgen deprivation therapy in management of prostate cancer: Study of testosterone-guided androgen Deprivation. Prostate 76 (2), 235–242. http://dx.doi.org/10.1002/pros.23117.

Osborne, C.K., Hobbs, K., Clark, G.M., 1985. Effect of estrogens and antiestrogens on growth of human breast cancer cells in athymic nude mice1. Cancer Res. 45, 584–590.

Page, S.T., Lin, D.W., Mostaghel, E.A., Hess, D.L., True, L.D., Amory, J.K., Nelson, P.S., Matsumoto, A.M., Bremner, W.J., 2006. Persistent intraprostatic androgen concentrations after medical castration in healthy men. J. Clin. Endocrinol. Metab. 91 (10), 3850–3856. http://dx.doi.org/10.1210/jc.2006-0968.

Pasetto, S., Enderling, H., Gatenby, R.A., Brady-Nicholls, R., 2022. Intermittent hormone therapy models analysis and Bayesian Model comparison for prostate cancer. Bull. Math. Biol. 84 (1), 2. http://dx.doi.org/10.1007/s11538-021-00953-w.

Phan, T., Crook, S.M., Bryce, A.H., Maley, C.C., Kostelich, E.J., Kuang, Y., 2020. Review: Mathematical modeling of prostate cancer and clinical application. Appl. Sci. 10 (8), 2721. http://dx.doi.org/10.3390/app10082721.

Sahoo, S., Mishra, A., Kaur, H., Hari, K., Muralidharan, S., Mandal, S., Jolly, M.K., 2021. A mechanistic model captures the emergence and implications of non-genetic heterogeneity and reversible drug resistance in ER+ breast cancer cells. NAR Cancer 3 (3), zcab027. http://dx.doi.org/10.1093/narcan/zcab027.

Stanbrough, M., Bubley, G.J., Ross, K., Golub, T.R., Rubin, M.A., Penning, T.M., Febbo, P.G., Balk, S.P., 2006. Increased expression of genes converting adrenal androgens to testosterone in androgen-independent prostate cancer. Cancer Res. 66 (5), 2815–2825. http://dx.doi.org/10.1158/0008-5472.CAN-05-4000.

Stewart, G.D., Ross, J.A., McLaren, D.B., Parker, C.C., Habib, F.K., Riddick, A.C., 2010. The relevance of a hypoxic tumour microenvironment in prostate cancer. BJU Int. 105 (1), 8–13. http://dx.doi.org/10.1111/j.1464-410X.2009.08921.x, _eprint: https://onlinelibrary.wiley.com/doi/pdf/10.1111/j.1464-410X.2009.08921.x.

Tilman, D., 1980. Resources: A graphical-mechanistic approach to competition and predation. Amer. Nat. 116 (3), 362–393. http://dx.doi.org/10.1086/283633, Publisher: The University of Chicago Press.

Titus, M.A., Schell, M.J., Lih, F.B., Tomer, K.B., Mohler, J.L., 2005. Testosterone and dihydrotestosterone tissue levels in recurrent prostate cancer. Clin. Cancer Res. 11 (13), 4653–4657. http://dx.doi.org/10.1158/1078-0432.CCR-05-0525.

Umekita, Y., Hiipakka, R.A., Kokontis, J.M., Liao, S., 1996. Human prostate tumor growth in athymic mice: inhibition by androgens and stimulation by finasteride. Proc. Natl. Acad. Sci. 93 (21), 11802–11807. http://dx.doi.org/10.1073/pnas.93.21.11802, Publisher: Proceedings of the National Academy of Sciences.

Watson, P.A., Arora, V.K., Sawyers, C.L., 2015. Emerging mechanisms of resistance to androgen receptor inhibitors in prostate cancer. Nat. Rev. Cancer 15 (12), 701–711. http://dx.doi.org/10.1038/nrc4016, Number: 12 Publisher: Nature Publishing Group.

West, J., You, L., Zhang, J., Gatenby, R.A., Brown, J.S., Newton, P.K., Anderson, A.R., 2020. Towards multidrug adaptive therapy. Cancer Res. 80 (7), 1578–1589. http://dx.doi.org/10.1158/0008-5472.CAN-19-2669.

Wibmer, A., Hricak, H., Gondo, T., Matsumoto, K., Veeraraghavan, H., Fehr, D., Zheng, J., Goldman, D., Moskowitz, C., Fine, S.W., Reuter, V.E., Eastham, J., Sala, E., Vargas, H.A., 2015. Haralick texture analysis of prostate MRI: utility for differentiating non-cancerous prostate from prostate cancer and differentiating prostate cancers with different Gleason scores. Eur. Radiol. 25 (10), 2840–2850. http://dx.doi.org/10.1007/s00330-015-3701-8.

Zhang, J., Cunningham, J.J., Brown, J.S., Gatenby, R.A., 2017. Integrating evolutionary dynamics into treatment of metastatic castrate-resistant prostate cancer. Nature Commun. 8 (1), 1816. http://dx.doi.org/10.1038/s41467-017-01968-5, Publisher: Nature Publishing Group.

Zhang, J., Cunningham, J., Brown, J., Gatenby, R., 2022. Evolution-based mathematical models significantly prolong response to abiraterone in metastatic castrate-resistant prostate cancer and identify strategies to further improve outcomes. eLife 11, e76284. http://dx.doi.org/10.7554/eLife.76284.

Zheng, J., 2012. Energy metabolism of cancer: Glycolysis versus oxidative phosphorylation (review). Oncol. Lett. 4 (6), 1151–1157. http://dx.doi.org/10.3892/ol.2012.928, arXiv: NIHMS150003 Publisher: Spandidos Publications ISBN: 1792-1074–r1792-1082.